

Self-consistent Evolution of Magnetic Fields and Chiral Asymmetry in the Early Universe

Alexey Boyarsky,^{1,2,3} Jürg Fröhlich,⁴ and Oleg Ruchayskiy⁵

¹*Instituut-Lorentz for Theoretical Physics, Universiteit Leiden, Niels Bohrweg 2, Leiden, The Netherlands*

²*Ecole Polytechnique Fédérale de Lausanne, FSB/ITP/LPPC, BSP 720, CH-1015, Lausanne, Switzerland*

³*Bogolyubov Institute of Theoretical Physics, Kyiv, Ukraine*

⁴*Institute of Theoretical Physics, ETH Hönggerberg, CH-8093 Zurich, Switzerland*

⁵*CERN Physics Department, Theory Division, CH-1211 Geneva 23, Switzerland*

We show that the evolution of magnetic fields in a primordial plasma, filled with Standard Model particles, at temperatures $T \gtrsim 10\text{MeV}$ is strongly affected by the quantum chiral anomaly – an effect that has been neglected previously. Although reactions equilibrating left and right-chiral electrons are in deep thermal equilibrium for $T \lesssim 80\text{TeV}$, an asymmetry between these particle develops in the presence of strong magnetic fields. This results in magnetic helicity transfer from shorter to longer scales. This also leads to an effective generation of lepton asymmetry that may survive in the plasma down to temperatures $T \sim 10\text{MeV}$, which may strongly affect many processes in the early Universe. Although we report our results for the Standard Model, they are likely to play an important role also in its extensions.

PACS numbers: 98.80.Cq; 07.55.Db

Magnetic fields are expected to play an important role in the early Universe. Recent observational indications of the presence of magnetic fields in the inter-galactic medium [1–3] suggest that cosmological magnetic fields (CMF) may survive even till the present epoch. Thus they could have played the role of seeds for the formation of galactic magnetic fields. A number of mechanisms for the creation of CMF at very high temperatures have been proposed (see e.g. [4–6] and refs. therein).

In this paper we concentrate, however, on a different problem: we *assume* that strong CMF were *already* generated at a temperature $\gtrsim 100\text{GeV}$ and we study the subsequent evolution of such fields. Usually, this evolution is described by the system of Maxwell plus Navier-Stokes equations (for a detailed review see [5, 7]). Here we will argue that, for temperatures $T \gtrsim 10\text{MeV}$, this system of MHD equations *should be extended to include a new effective degree of freedom*, even if all particles and reactions are described by just the Standard Model of particle physics. This significantly affects the evolution of CMF and the state of the primordial plasma.

At such temperature rates, of all perturbative processes related to the electron’s finite mass are suppressed as $(m_e/T)^2$. Ignoring these corrections for a moment, the number of left and right-chiral electrons¹ is conserved independently.² That is, apart from the vector current $j^\mu = \bar{\psi}\gamma^\mu\psi$ describing conservation of electric charge ($n_L + n_R$), the average number density of the left- (right) chiral electrons $n_{L,R} = \frac{1}{2V} \int d^3x \psi^\dagger(1 \pm \gamma_5)\psi$ does not

change with time. This is true on time scales smaller than the *chirality-flipping scale* Γ_f^{-1} . Although the chirality-flipping rate is suppressed as compared to the rate of chirality-preserving weak and electromagnetic processes, it is faster than the Hubble expansion rate, $H(T)$, for temperatures below 80TeV [8] and chirality flipping processes are in thermodynamic equilibrium. Yet on time scales $\Gamma_{EM,weak}^{-1} < t < \Gamma_f^{-1}$ one should introduce independent chemical potentials, μ_L and μ_R , for two approximately conserved number densities, with $n_{L,R} = \frac{\mu_{L,R}}{6}T^2$. In the presence of external *classical* fields the conservation of the axial current is spoiled, however, by the *chiral anomaly* [9] – a quantum effect leading to a change of $n_L - n_R$:

$$\frac{d(n_L - n_R)}{dt} = \frac{2\alpha}{\pi} \frac{1}{V} \int d^3x E \cdot B = -\frac{\alpha}{\pi} \frac{d\mathcal{H}}{dt}, \quad (1)$$

where $\alpha = \frac{e^2}{4\pi}$ is the fine-structure constant and \mathcal{H} is the *magnetic helicity* defined as

$$\mathcal{H}(t) = \frac{1}{V} \int_V d^3x A \cdot B, \quad (2)$$

(where B is the magnetic field and A the vector potential, with $B = \nabla \times A$). The quantity (2) is gauge invariant, provided that B is parallel to the boundary of V (see e.g. [7]). The time evolution of $\mathcal{H}(t)$ is given by [7]

$$\frac{d\mathcal{H}}{dt} = -\frac{2}{V} \int_V d^3x E \cdot B. \quad (3)$$

In terms of the difference of left and right chemical potentials, $\Delta\mu \equiv \mu_L - \mu_R$, Eq. (1) reads

$$\frac{d(\Delta\mu)}{dt} = -\frac{c_\Delta\alpha}{T^2} \frac{d\mathcal{H}(t)}{dt}, \quad (4)$$

where c_Δ is a numerical coefficient of order one that describes the dependence of n_L on globally conserved charges in the primordial plasma.

¹ More precisely, n_L is the *difference* between the number of left particles and left anti-particles (same for n_R).

² The number of left-chiral electrons is not conserved when weak processes are fast (the conserved quantities are $n_L + n_{\nu_e}$ and n_R). The coefficient c_Δ in Eq. (4) below takes this into account.

If $\Delta\mu \neq 0$, the chiral anomaly leads to an additional contribution to the current in Maxwell's equations [10–17]:

$$\nabla \times B = \sigma E + \frac{\alpha}{\pi} \Delta\mu(t) B ,$$

or, combining it with the Bianchi identity $\nabla \times E = -\dot{B}$:

$$\frac{\partial B}{\partial t} = \frac{1}{\sigma} \nabla^2 B + \frac{\alpha}{\pi} \frac{\Delta\mu}{\sigma} \nabla \times B . \quad (5)$$

As weak reactions are fast enough at these temperatures to establish local thermodynamic equilibrium (LTE), in the background of long-wavelength electromagnetic fields, space-dependent chemical potentials $\mu_{L,R}(x)$ may be defined. Eqs. (1), (4) can then be written in a local form, and Eq. (5) acquires additional terms, proportional to the gradients of $\Delta\mu(x)$ [13, 15, 16]. We assume fields to be slowly varying and neglect these effects as well as those depending on the velocity field. We will show that, even in this limit, the evolution of magnetic fields significantly changes as compared to the usual Maxwell equations. A more realistic analysis should include all the derivative terms, as well as the Navier-Stokes equation describing, in particular, turbulent effects known to be important for the evolution of CMF. We leave a more complete microscopic derivation and an analysis of the full system to future work and use the simple model described above to illustrate the previously neglected effects.

Eqs. (4–5) remain valid in an expanding Universe if written in conformal coordinates (see e.g. [5, 11, 18]). Henceforth we use conformal quantities and define conformal time as $\eta = \frac{M_*}{T}$, where $M_* = \sqrt{\frac{90}{8\pi^3 g_*}} M_{Pl}$ and g_* is the effective number of relativistic degrees of freedom.

Eqs. (4–5) are translation and rotation invariant. We introduce the *magnetic helicity density*, \mathcal{H}_k , and the *magnetic energy density*, ρ_k , in Fourier-space, with $\rho_B(\eta) = \int dk \rho_k(\eta)$ and $\mathcal{H}(\eta) = \int dk \mathcal{H}_k(\eta)$.³ The quantities \mathcal{H}_k and ρ_k obey the inequality $|\mathcal{H}_k| \leq \frac{2}{k} \rho_k$, which is saturated for field configurations known as *maximally helical fields*. In our subsequent analysis, we focus on this case and *choose for definiteness* $\mathcal{H}_k > 0$ and $\Delta\mu > 0$. Multiplying the Fourier version of Eq. (5) by the complex-conjugate mode \vec{B}_k^* , we obtain, after some simple manipulations (see Appendix E for details, cf. [19]),

$$\frac{\partial \mathcal{H}_k}{\partial \eta} = -\frac{2k^2}{\sigma_c} \mathcal{H}_k + \frac{\alpha}{\pi} \frac{k \Delta\mu}{\sigma_c} \mathcal{H}_k , \quad (6)$$

$$\frac{d(\Delta\mu)}{d\eta} = -(c_\Delta \alpha) \int dk \frac{\partial \mathcal{H}_k}{\partial \eta} - \Gamma_f \Delta\mu , \quad (7)$$

where we have restored the chirality flipping rate Γ_f in Eq. (7) and used the conductivity $\sigma_c \equiv \sigma(\eta)/T \approx 70$ [21].

The system (6–7) has been previously studied in two regimes. It was demonstrated in [11, 16, 22] that, in the presence of a large initial chemical potential difference $\Delta\mu(\eta) > 0$, the quantity

$$\mathcal{H}_k(\eta) = \mathcal{H}_k^0 \exp \left\{ \frac{2k}{\sigma_c} \left(\frac{\alpha}{2\pi} \int_{\eta_0}^{\eta} \Delta\mu(\tilde{\eta}) d\tilde{\eta} - k(\eta - \eta_0) \right) \right\} \quad (8)$$

grows exponentially fast for sufficiently long wavelengths. Conversely, in [13] the initial background of helical (hyper)magnetic fields was used to generate a non-zero chemical potential for $T > 100$ GeV.

In this work, however, we consider helical CMF with some initial spectrum \mathcal{H}_k^0 , already present at $T \sim 100$ GeV in the hot plasma, filled with particles in thermal equilibrium (cf. [18–20, 23]). It was believed that as $\Gamma_f \gg H(T)$ for $T \lesssim 80$ TeV, no chiral asymmetry will survive.

Chirality evolution. *Below we show that both $\Delta\mu$ and the magnetic helicity do survive below 100 GeV on time-scales much longer than diffusion or chirality flipping times (till $10 \div 100$ MeV).* (For $\Gamma_f \rightarrow 0$ the system (6–7) can even reach a stationary state with non-zero B and $\Delta\mu$).

To see this, it is convenient to separate on the right hand side of Eq. (7) a source term $S_B(\eta)$ (independent of $\Delta\mu$) (cf. [13]):

$$\frac{d(\Delta\mu)}{d\eta} = -(\Gamma_B(\eta) + \Gamma_f) \Delta\mu + S_B(\eta) , \quad (9)$$

where

$$\begin{aligned} \Gamma_B(\eta) &\equiv \frac{c_\Delta \alpha^2}{\pi \sigma_c} \int dk k \mathcal{H}_k = \frac{2c_\Delta \alpha^2}{\pi \sigma_c} \rho_B , \\ S_B(\eta) &\equiv 2 \frac{c_\Delta \alpha}{\sigma_c} \int dk k^2 \mathcal{H}_k . \end{aligned} \quad (10)$$

We begin our analysis of Eqs. (6) and (9–10) with the case where $\Gamma_f = 0$ and the field is *initially “monochromatic”*, i.e.,

$$\mathcal{H}_k(\eta) = \mathcal{H}(\eta) \delta(k - k_0) . \quad (11)$$

The form (11) is preserved during the evolution as Eq. (6) is homogeneous.⁴ Putting in Eq. (9) $d(\Delta\mu)/d\eta = 0$ and $\Gamma_f = 0$ we find the so-called *tracking solution*:

$$\Delta\mu_{\text{tr}} = \frac{S_B(\eta)}{\Gamma_B(\eta)} = \frac{2\pi k_0}{\alpha} . \quad (12)$$

This is an *exact static* solution of the system (6), (9): $\Delta\mu_{\text{tr}}$ and $\mathcal{H}(\eta)$ remain constant, i.e., dissipation due to

³ In terms of left and right circular polarized modes B_k^\pm , $\mathcal{H}_k = \frac{k}{2\pi^2} (|B_k^+|^2 - |B_k^-|^2)$ and $\rho_k = \frac{k^2}{(2\pi)^2} (|B_k^+|^2 + |B_k^-|^2)$. Integrals over k run over the radial direction only (see e.g. [18–20]).

⁴ This is an artifact of our homogeneous approximation (4–5), with $\Delta\mu$ independent on spatial coordinates, see below.

magnetic diffusion is *exactly compensated* by growth due to a non-vanishing chemical potential difference $\Delta\mu_{\text{tr}}$; (cf. (8)).

Until now we have completely neglected the massiveness of the electrons. It is straightforward to compute that the rate $\Gamma_f(\eta)$ due to electromagnetic processes is:⁵ $\Gamma_f(\eta) \approx \alpha^2 \left(\frac{m_e}{3M_*}\right)^2 \eta^2$. Eqs. (6), (9) can be rewritten to describe deviations from the equilibrium static solution (12):

$$\frac{d\Delta\mu}{d\eta} = -\Gamma_B(\Delta\mu - \Delta\mu_{\text{tr}}) - \Gamma_f\Delta\mu, \quad (13)$$

$$\frac{d\Gamma_B}{d\eta} = \frac{\Gamma_B}{\eta_\sigma} \left(\frac{\Delta\mu}{\Delta\mu_{\text{tr}}} - 1 \right), \quad (14)$$

where $\eta_\sigma \equiv \frac{2k^2}{\sigma_c}$ is the *magnetic diffusion time*. From Eq. (13) we see that Γ_B and Γ_f , which enter symmetrically in Eq. (9), play very different roles. The rate Γ_f , that depends *only* on temperature, constantly drives $\Delta\mu$ to zero. The Γ_B term pushes the system towards the equilibrium value (12) (that depends only on k_0). It depends on ρ_B and has its own dynamics, Eq. (14).

If the magnetic field is large (such that $\Gamma_B \gg \Gamma_f$), any initial value of $\Delta\mu$ will be quickly “forgotten” and $\Delta\mu$ will be driven towards $\Delta\mu_{\text{tr}}$. At that moment a new tracking solution will take over, with $\Delta\mu - \Delta\mu_{\text{tr}} \approx \gamma\Delta\mu_{\text{tr}}$, where

$$\gamma(\eta) \equiv \frac{\Gamma_f(\eta)}{\Gamma_B(\eta)}. \quad (15)$$

This new solution is valid, provided two conditions hold: (i) $\gamma \ll \Gamma_B t$ and (ii) $\gamma \ll \Gamma_B \eta_\sigma$. When this holds the evolution of Γ_B is given by (14).

$$\frac{d\Gamma_B}{d\eta} = -\frac{\gamma(\eta)}{\eta_\sigma} \Gamma_B = -\frac{1}{\eta_\sigma} \Gamma_f(\eta). \quad (16)$$

Eq. (16) shows that Γ_B remains practically constant when $\eta \ll \eta_\sigma/\gamma(\eta)$, which is *significantly longer* than η_σ , as $\gamma \ll 1$. To estimate the time at which the function $\gamma(\eta) \sim 1$ we note that it evolves with time because of an increasing chirality flipping rate $\Gamma_f(\eta) \propto \eta^2$ and because the total magnetic energy dissipates (16). Neglecting this latter change, we estimate γ to be given by:

$$\gamma = \frac{\pi\sigma_c}{2c_\Delta} \left(\frac{m_e}{3M_*}\right)^2 \frac{\eta^2}{\frac{\pi^2}{30}g_* r_B} = \frac{10^{-5}}{r_B} \left(\frac{100 \text{ MeV}}{T}\right)^2 \left(\frac{30}{g_*}\right), \quad (17)$$

where we used $r_B \equiv \rho_B/(\frac{\pi^2}{30}g_*T^4)$ is the fraction of magnetic energy density to the total energy density. From

Eq. (16) we see in addition that Γ_B remains approximately constant as long as $\frac{1}{\eta_\sigma} \int \gamma(\eta)d\eta < 1$. Using (17) we find that (this is illustrated in Fig. A1 in Appendix A).

$$\frac{\gamma(\eta)\eta}{3\eta_\sigma} \leq 1. \quad (18)$$

Inverse cascade. So far we have considered a toy model example of “monochromatic” helical field (11). Although the Eq. (6) is linear, the modes \mathcal{H}_k are not independent for different k (due to the integral in the Eq. (7)). For a continuous spectrum, this interaction results in another very important effect: the initial spectrum reddens with time, the total helicity being conserved (similarly to the “*inverse cascade*” phenomenon [7], Sec. 7.2.3).

Indeed, let us consider first the case of two modes ($k_1, \mathcal{H}_1(\eta)$) and ($k_2, \mathcal{H}_2(\eta)$) with $k_1 > k_2$, to understand the situation qualitatively. While $\Gamma_B \gg \Gamma_f$, the evolution for $\Delta\mu$ has the form:

$$\frac{d(\Delta\mu)}{d\eta} = -\frac{c_\Delta\alpha^2}{\pi\sigma_c} \left(k_1\mathcal{H}_1 + k_2\mathcal{H}_2\right)\Delta\mu + \frac{2c_\Delta\alpha}{\sigma_c} \left(k_1^2\mathcal{H}_1 + k_2^2\mathcal{H}_2\right). \quad (19)$$

One can again try to construct a tracking solution of Eq. (19) by putting its l.h.s. to zero. It is clear, however, that, unlike in the case (12), such a tracking solution cannot be time independent. Indeed, according to Eq. (6) $\dot{\mathcal{H}}_k = 0$ only if $\Delta\mu = \frac{2\pi k}{\alpha}$, while our solution $\Delta\mu_{\text{tr}} = \frac{2\pi}{\alpha} \frac{k_1^2\mathcal{H}_1 + k_2^2\mathcal{H}_2}{k_1\mathcal{H}_1 + k_2\mathcal{H}_2}$ depends on both modes. In the case where a shorter mode (k_1) contains most of the energy density, $\Delta\mu$ will grow very fast and reach: $\Delta\mu_{\text{tr}} \approx \frac{2\pi k_1}{\alpha}(1 - \epsilon)$. Initially $\epsilon = \frac{k_2\mathcal{H}_2}{k_1\mathcal{H}_1} \ll 1$ as \mathcal{H}_2 is subdominant and $\Delta\mu$ is close to its “static” value for k_1 . Therefore the mode \mathcal{H}_1 remains almost constant, for $\eta < \eta_\sigma(k_1)/\epsilon(\eta)$. For the mode \mathcal{H}_2 , however, $k_2 < \frac{\alpha\Delta\mu_{\text{tr}}}{2\pi}$ and from the solution (8) (valid for any $\Delta\mu(\eta)$) we see that \mathcal{H}_2 will start growing. As its growth enters the exponential phase, ϵ increases and k_1 becomes *greater than* $\Delta\mu(\eta)$, causing \mathcal{H}_1 to decay exponentially. $\Delta\mu(\eta)$ will therefore quickly evolve to the value $\frac{2\pi}{\alpha}k_2$. From Eq. (6) we find that for $\epsilon \ll 1$:

$$\mathcal{H}_2(\eta) \approx \mathcal{H}_2(\eta_0)e^{\frac{2k_1k_2}{\sigma_c}\eta} \quad (20)$$

and see that $\dot{\mathcal{H}}_1 = -\dot{\mathcal{H}}_2$ as long as $\Gamma_B \gg \Gamma_f$, i.e. the total helicity of the system is conserved.⁶

The evolution of continuous spectra is qualitatively very similar. Assume that the initial helicity spectrum \mathcal{H}_k^0 has its maximum at a scale k_1 and then decays as $\mathcal{H}_k^0 \propto \left(\frac{k}{k_1}\right)^{n_s-2}$, with $n_s \geq 3$. The scale k_1 determines the value of $\Delta\mu$ at the beginning, while the longer modes

⁵ The contribution of weak processes to Γ_f is small at $T < 100 \text{ GeV}$, see Appendix D.

⁶ $\dot{\mathcal{H}}$ is related to $\Delta\mu$ by Eq. (4). Even if $\Delta\mu$ changes smoothly, the very small numerical coefficient in (4) suppresses the change of \mathcal{H} .

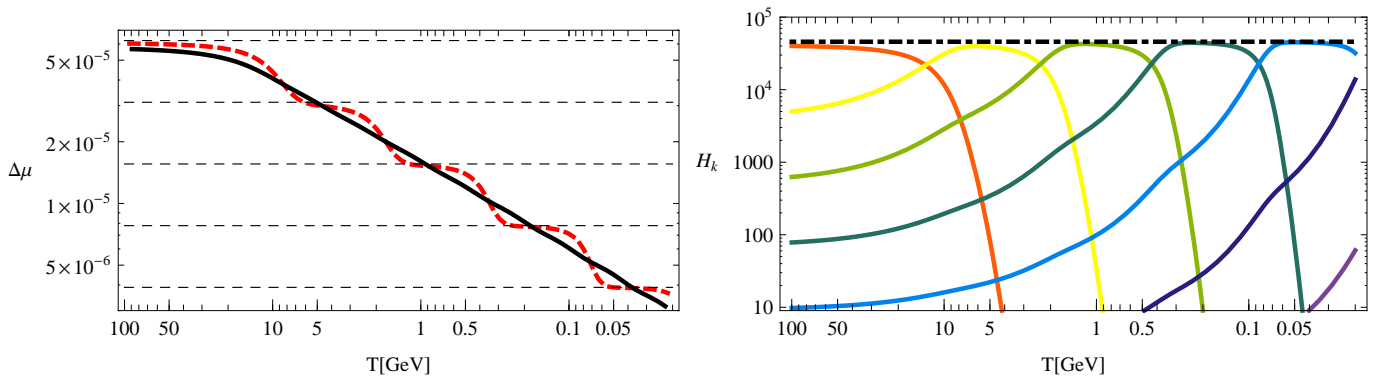


FIG. 1: Evolution in the absence of chirality flip for continuous spectrum $\mathcal{H}_k^0 \propto k^3$. **Left:** the evolution of $\Delta\mu(\eta)$ (black solid line). The red dashed line: the approximation of the spectrum by 10 modes ($k_n = 10^{-10} \times 2^{n-1/2}$, $n = 1, 10$). The horizontal lines are tracking solutions for individual modes k_n . **Right:** transfer of helicity from the shorter to the longer modes (red to blue).

grow. At the moment when back-reaction of these growing modes on $\Delta\mu$ becomes non-negligible, the chemical potential difference gets smaller and the modes with $k_1 \gtrsim k > \frac{\alpha\Delta\mu(\eta)}{2\pi}$ start decaying.

For discrete spectrum $\Delta\mu$ changes by “steps”, defined by the modes k_n (see Fig. 1 for $\Gamma_f = 0$, red dashed curve). Every such “step” corresponds, on the other panel of Fig. 1, to a fast decay of one helicity mode and exponential growth of an adjacent one (from red to purple), while the total helicity remains constant (black dot-dashed line). The conservation of helicity implies that the total magnetic energy gets dissipated as $\rho_k = \frac{k}{2}\mathcal{H}_k$ for helical fields. If we sample the same spectrum with a larger number of modes, the evolution of $\Delta\mu$ becomes monotone. If the initial spectrum is sharp ($n_s > 3$), $\Delta\mu$ will decay more slowly, and the short modes will survive for a longer time. The resulting spectrum will, however, be roughly the same – the helicity concentrates around the longest mode k_2 that had enough time to start growing, $\Delta\mu = \Delta\mu_{\text{tr}}(k_2)$, the magnetic energy is smaller by the factor $\frac{k_2}{k_1}$. We believe that these results correctly describe the interaction between different helicity modes even in the inhomogeneous case, provided that deviations from LTE are not very dramatic and $\Delta\mu(x)$ is smooth.

Finally, the exact numerical solution of the full system with continuous spectrum and finite $\gamma(\eta)$ is shown in Fig. 2 where the red dashed line shows $\Delta\mu(\eta)$ in the case $\Gamma_f = 0$ and the thick blue and green lines show $\Delta\mu(\eta)$ for $\Gamma_f \neq 0$ and different r_B . This full evolution follows that of $\Gamma_f = 0$ and then breaks down exponentially fast when $\gamma(\eta) \sim 1$ and (18) holds.

Conclusion. This work demonstrates that the *traditional MHD equations should be modified*, when applied to a plasma of relativistic particles with $T \gg m$. The proper account of the *chiral anomaly* changes the evolution of magnetic fields in two ways: (i) the magnetic fields survive several orders of magnitude longer than the time defined by magnetic diffusion (Eqs. (16)–(17)) and

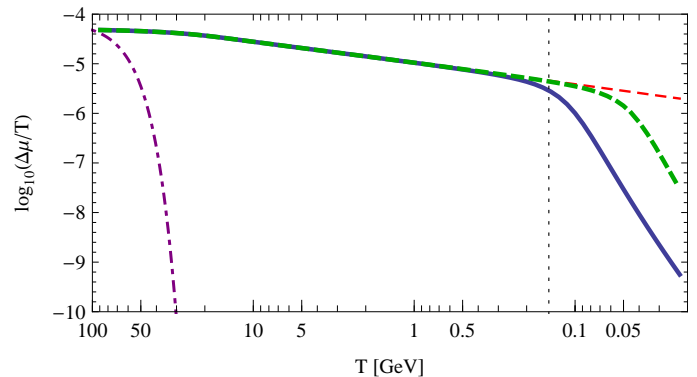


FIG. 2: Evolution of the chemical potential for $r_B = 5 \times 10^{-5}$ (solid blue line). Vertical line at $T \approx 150$ MeV marks $\gamma = 1$, $\Delta\mu(150 \text{ MeV}) \simeq 2.9 \times 10^{-6}$. The red dashed line shows evolution of the chemical potential for $\Gamma_f = 0$. The green short-dashed line shows $\Delta\mu(\eta)$ for $r_B = 5 \times 10^{-4}$. The purple dashed-dotted line shows the decay of the chemical potential in the absence of magnetic field.)

(ii) an “inverse cascade” develops, transferring energy from shorter to longer wavelength modes. The effect depends on the energy of magnetic fields parametrized by its ratio to the total energy density, r_B . In the literature discussing the evolution of magnetic fields (see e.g. [18, 20, 23]) $r_B \leq 1$ is often considered. It was demonstrated e.g. in Refs. [24, 25] that $r_B \sim \text{few} \times 10^{-3}$ may be generated at cosmological first order phase transitions. The mechanism of [26] predicts maximally helical magnetic fields with $B \sim 100 \text{ GeV}^2$ (i.e. $r_B \sim 10^{-2}$, c.f. [27]) at small scales. See [6, 24–26, 28, 29] and refs. therein.

We refer to the value of r_B at $T \sim 100 \text{ GeV}$. Due to the inverse cascade and helicity conservation this energy decreases by about an order of magnitude by the time when our effect stops ($T \sim 10 - 100 \text{ MeV}$). The subsequent evolution of the magnetic fields is described by

the conventional MHD [5, 18, 19], a significant part of r_B further dissipates, so that only the large scale tail of the spectrum may survive due to turbulent effects. To predict the final fate of these CMF for every initial spectrum and compare them with cosmological bounds (see e.g. [30]), our results should be combined with the MHD analysis. Nevertheless, the above-described mechanism, based *entirely on the Standard Model*, clearly improves the chances of survival of CMF generated at subhorizon scales [31]. Indeed, even for $r_B \sim 10^{-5}$ the fields survive down to $T \sim 100$ MeV, while for $r_B \sim 0.1$ the inverse cascade is operational down to $T \sim 10$ MeV. Moreover,

regardless of the survival of the CMF, this effect is important as the left-right asymmetry in the electron sector survives down to $T \sim \mathcal{O}(100)$ MeV and thus potentially affects important processes in the early Universe: can change the nature of the QCD phase transition [32] and produce gravitational waves [33], leave its imprints on BBN and CMB [34, 35].

Acknowledgments. We would like to thank V. Cheianov, B. Pedrini, and M. Shaposhnikov for useful discussions.

-
- [1] A. Neronov and I. Vovk, *Science* **328**, 73 (2010).
- [2] K. Dolag, M. Kachelriess, S. Ostapchenko, and R. Tomas, *Astrophys. J.* **727**, L4 (2011).
- [3] F. Tavecchio et al., *Mon. Not. Roy. Astron. Soc.* **406**, L70 (2010).
- [4] D. Grasso and H. R. Rubinstein, *Phys. Rept.* **348**, 163 (2001).
- [5] M. Giovannini, *Int. J. Mod. Phys.* **D13**, 391 (2004).
- [6] A. Kandus, K. E. Kunze, and C. G. Tsagas, *Phys. Rept.* **505**, 1 (2011).
- [7] D. Biskamp, *Nonlinear Magnetohydrodynamics*, Cambridge monographs on plasma physics (Cambridge University Press, 1997), ISBN 9780521599184.
- [8] B. A. Campbell, S. Davidson, J. R. Ellis, and K. A. Olive, *Phys. Lett.* **B297**, 118 (1992).
- [9] S. Treiman, R. Jackiw, E. Witten, and B. Zumino, *Current algebra and anomalies*, Princeton series in physics (Princeton University Press, 1985), ISBN 9780691083988.
- [10] A. Vilenkin, *Phys. Rev.* **D22**, 3080 (1980).
- [11] M. Joyce and M. E. Shaposhnikov, *Phys. Rev. Lett.* **79**, 1193 (1997).
- [12] A. N. Redlich and L. C. R. Wijewardhana, *Phys. Rev. Lett.* **54**, 970 (1985).
- [13] M. Giovannini and M. E. Shaposhnikov, *Phys. Rev.* **D57**, 2186 (1998).
- [14] A. Y. Alekseev, V. V. Cheianov, and J. Frohlich, *Phys. Rev. Lett.* **81**, 3503 (1998).
- [15] J. Fröhlich and B. Pedrini, in *Mathematical Physics 2000*, edited by A. S. Fokas, A. Grigoryan, T. Kibble, and B. Zegarlinski (World Scientific Publishing Company, 2000), International Conference on Mathematical Physics 2000, Imperial college (London), hep-th/0002195.
- [16] J. Fröhlich and B. Pedrini, in *Statistical Field Theory*, edited by A. Cappelli and G. Mussardo (Kluwer, 2002), cond-mat/0201236.
- [17] K. Fukushima, D. E. Kharzeev, and H. J. Warringa, *Phys. Rev.* **D78**, 074033 (2008).
- [18] R. Banerjee and K. Jedamzik, *Phys. Rev.* **D70**, 123003 (2004).
- [19] L. Campanelli, *Phys. Rev. Lett.* **98**, 251302 (2007).
- [20] R. Banerjee and K. Jedamzik, *Phys. Rev. Lett.* **91**, 251301 (2003).
- [21] G. Baym and H. Heiselberg, *Phys. Rev.* **D56**, 5254 (1997).
- [22] V. B. Semikoz and D. D. Sokoloff, *Astronomy & Astrophysics* **433**, L53 (2004).
- [23] K. Jedamzik and G. Sigl, *Phys. Rev.* **D83**, 103005 (2011).
- [24] G. Baym, D. Bodeker, and L. D. McLerran, *Phys. Rev.* **D53**, 662 (1996).
- [25] G. Sigl, A. V. Olinto, and K. Jedamzik, *Phys. Rev.* **D55**, 4582 (1997).
- [26] T. Vachaspati, *Phys. Lett.* **B265**, 258 (1991).
- [27] Y.-Z. Chu, J. B. Dent, and T. Vachaspati, 1105.3744 (2011).
- [28] C. J. Copi, F. Ferrer, T. Vachaspati, and A. Achúcarro, *Phys. Rev. Lett.* **101**, 171302 (2008).
- [29] S. Davidson, *Phys. Lett.* **B380**, 253 (1996).
- [30] T. Kahniashvili, A. G. Tevzadze, S. K. Sethi, K. Pandey, and B. Ratra, *Phys. Rev.* **D82**, 083005 (2010).
- [31] R. Durrer and C. Caprini, *JCAP* **0311**, 010 (2003).
- [32] D. J. Schwarz and M. Stuke, *JCAP* **0911**, 025 (2009).
- [33] R. Durrer, *J. Phys. Conf. Ser.* **222**, 012021 (2010).
- [34] J. Lesgourgues and S. Pastor, *Phys. Rev. D* **60**, 103521 (1999).
- [35] G. Mangano, G. Miele, S. Pastor, O. Pisanti, and S. Sarikas, *JCAP* **1103**, 035 (2011).

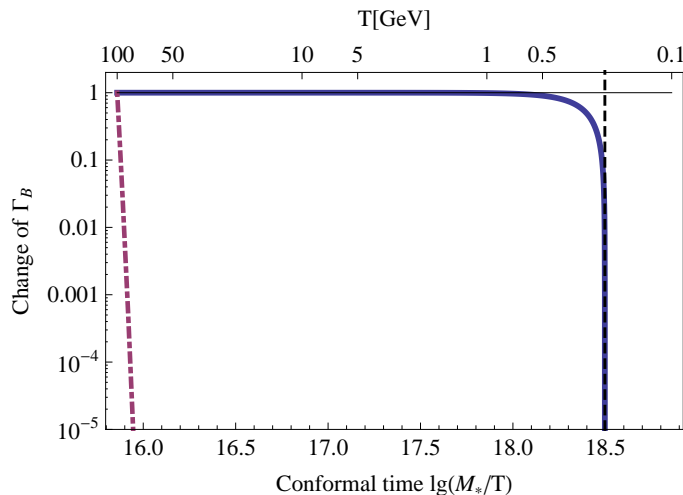


FIG. A1: The relative change of helicity (solid line) as compared to the solution of (16) (dashed line). The dot-dashed line shows the evolution of Γ_B in the absence of chemical potential (solely due to magnetic diffusion with $\lg(\eta_\sigma) \approx 16.1$). A black dashed-dotted line shows the evolution of $\gamma(\eta)$, growing at η^2 at small times and then starting to increase exponentially fast. A thin black vertical line marks the solution of (18).

Supplementary material

Appendix A: Evolution of a single mode

This Appendix provides numerical results, illustrating analytic results (14), (16), and (18). Fig. A1 shows the relative change of Γ_B from its initial value and the evolution of $\gamma(\eta)$. We see that for $\gamma \ll 1$ the value of Γ_B (i.e. the total energy density of the CMF) decays over a much longer time, η_σ/γ , than that of magnetic diffusion, and, a significantly positive value of the chemical potential (which would decay in the absence of magnetic field in a time $\eta \sim \Gamma_f^{-1}$) is maintained during this time.

The evolution of the mode is therefore similar to the one discussed above, as long as $\gamma \ll 1$. For $\gamma \sim 1$ the evolution quickly becomes that of standard MHD without a difference of chemical potentials, with Γ_B decaying due to magnetic diffusion and $\Delta\mu$ dissipating through perturbative flipping.

Appendix B: Evolution of several discrete modes ($\Gamma_f = 0$)

1. Analytic estimate of the time of the energy/helicity transfer between two modes

The results for the time of transfer of the energy and helicity between two modes can be derived in a different way than done in the main text. Namely, consider the initial spectrum

$$H(\eta_0) = H_1^0 \delta(k - k_1) + H_2^0 \delta(k - k_2) \quad (\text{B1})$$

The spectrum preserves its shape throughout evolution and the tracking solution of Eq. (19) is given by

$$\Delta\mu_{\text{tr}}(\eta) \approx \frac{2\pi k_1^2 H_1 + k_2^2 H_2}{\alpha k_1 H_1 + k_2 H_2} \quad (\text{B2})$$

In the presence of such a $\Delta\mu$, the two modes in (B1) evolve as follows:

$$\dot{H}_1 = -\frac{2k_1 k_2}{\sigma_c} \frac{k_1 - k_2}{k_1 H_1 + k_2 H_2} H_1 H_2 \quad , \quad \dot{H}_2 = -\dot{H}_1 \quad (\text{B3})$$

To see how fast the helicity (energy) gets transferred from the mode k_1 to k_2 let us combine two equations (B3) into a single equation for the ratio $h(\eta) = H_1(\eta)/H_2(\eta)$ (such that $h(\eta_0) = h_i > 1$ and $h(\eta) \rightarrow 0$ as $t \rightarrow \infty$):

$$\frac{dh}{dt} = -\frac{2k_1^2}{\sigma} q(1 - q) \frac{h(1 + h)}{h + q} \quad (\text{B4})$$

(where $q = k_2/k_1 < 1$). As a result we can obtain the time difference for h to change from h_i to h :

$$\Delta t = \frac{\sigma}{2k_1^2} \left[\frac{1}{1-q} \log \frac{h_i}{h} + \frac{1}{q} \log \frac{1+h_i}{1+h} \right] \quad (\text{B5})$$

We can see that the time when helicities of both modes equalize (i.e. $h(\eta) = 1$) is given by

$$\Delta t_H = \frac{\sigma}{2k_1^2} \left[\frac{\log h_i}{1-q} + \frac{1}{q} \log \frac{1+h_i}{2} \right] \quad (\text{B6})$$

From Eq.(B5) one can also easily determine the time when the energies of two modes equalize (i.e. when $h = \frac{1}{q}$).

In the case when two modes with very different wave numbers (i.e. when $q \ll 1$), the time Δt_H is approximately equal to

$$\Delta t_H \approx \frac{\sigma}{2k_1^2} \frac{1}{q} \log h_i = \frac{2\pi\sigma}{k_1 k_2} \log h_i \quad (\text{B7})$$

Notice, that this time is much longer than the magnetic diffusion time $\frac{\sigma}{2k_1^2}$ and it depends on the ratio of initial amplitudes only logarithmically.

2. Approximations, used in derivation of Eq. (20)

In this Section we provide some details regarding the derivation, used in the main paper and leading to Eq. (20). Consider the system of Eqs. (19). Let us assume that $k_1 H_1(\eta_0) \gg k_2 H_2(\eta_0)$ and $k_2 < k_1$. Then, we can rewrite the tracking solution (B2) as

$$\Delta\mu_{\text{tr}} \approx \frac{2\pi k_1}{\alpha} (1 - \epsilon) \quad (\text{B8})$$

(where $\epsilon = \frac{k_2 H_2}{k_1 H_1} \ll 1$). Its time evolution is given by

$$\frac{d\Delta\mu}{dt} = -\Gamma_B \left(\Delta\mu - \frac{2\pi k_1}{\alpha} (1 - \epsilon(\eta)) \right) \quad (\text{B9})$$

The evolution of two modes H_1 and H_2 is then given by

$$\dot{H}_1 = -\frac{\epsilon(\eta)}{t_{\sigma 1}} H_1 = -\frac{k_2}{k_1 t_{\sigma 1}} H_2 \quad (\text{B10})$$

and

$$\dot{H}_2 = \frac{H_2}{t_{\sigma 2}} \left(\frac{k_1(1 - \epsilon(\eta))}{k_2} - 1 \right) \quad (\text{B11})$$

from which it follows that

$$H_2(\eta) = H_2(\eta_0) e^{\frac{k_1}{k_2} \frac{\eta}{t_{\sigma 2}}} \quad (\text{B12})$$

This result is confirmed by numerical solution in Fig. B2, where the solution of Eq. (B12) is shown in black dot-dashed line (see also B1). From here we can find the equation for $\dot{\Gamma}_B$:

$$\dot{\Gamma}_B = \left(\frac{2c_\Delta \alpha^2}{\pi \sigma_c} \right) \frac{k_1 - k_2}{\sigma_c} k_1 k_2 H_2 \quad (\text{B13})$$

3. Evolution of several discrete modes

The evolution of 10 modes, sampling a continuous spectrum with $\mathcal{H}_k^0 \propto k^3$ without perturbative chirality flip (solid lines in Fig. B1) and its comparison with the evolution of the same spectrum but for two modes only with the same helicities initially stored in each mode – short-dashed lines in Fig. B1. Fig. B2 compares the exact numerical solution of the case with two modes only (red and blue lines) with the result (20) of the approximate (in $\mathcal{H}_{k_2}/\mathcal{H}_{k_1}$) approximation (black dot-dashed line).

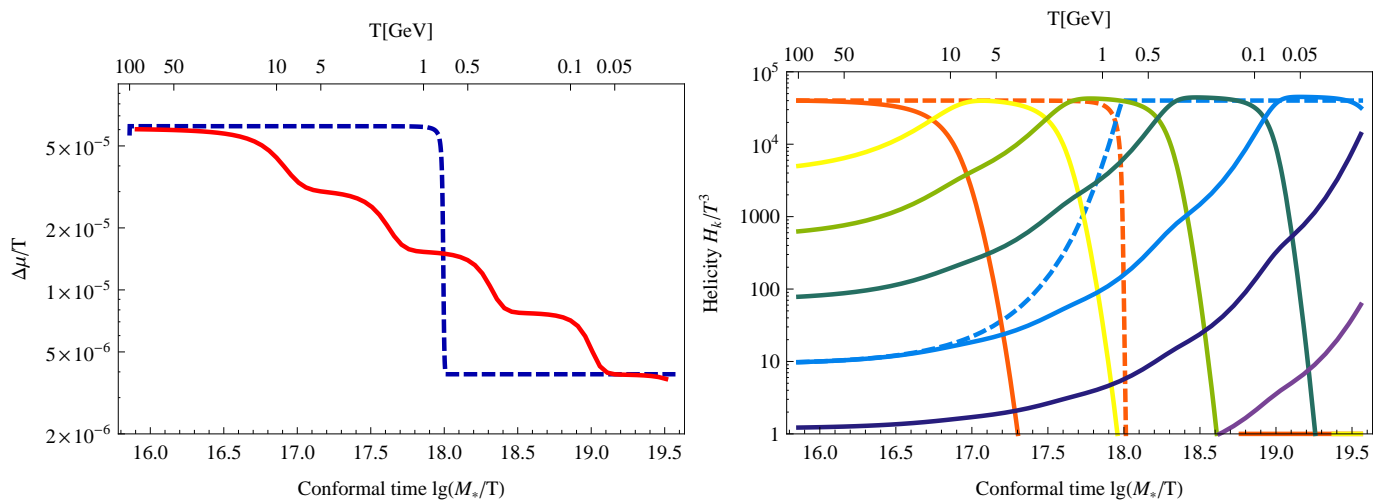


FIG. B1: Comparison between evolution of chemical potential (left) and helicity modes (right) for 10 modes (solid lines) and 2 modes (1st and 5th of the previous set) – dashed lines.

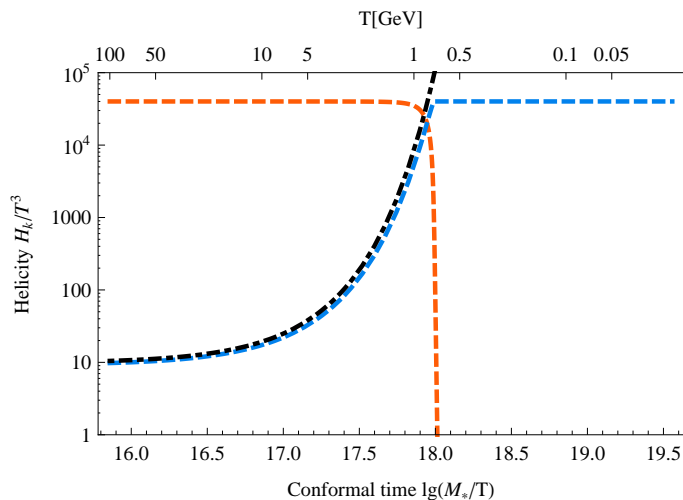


FIG. B2: Comparison of the evolution of a long-wavelength mode (in the 2 mode solution shown in Fig.B1) with its linear approximation, given by Eq. (20) – dashed-dotted black line.

Appendix C: Inverse cascade and the shape of the resulting spectrum

In the case of the continuous spectrum while $\gamma \ll 1$ the evolution is identical to the case of $\Gamma_f = 0$, described above (see Fig. 2). The condition $\gamma(\eta) \leq 1$ determines the time over which the described effect is present in plasma. We see from Eq. (17) that for $r_B \gtrsim 10^{-5}$ the fields, generated very early (probably at $T_0 \sim 100$ GeV) can survive until $T \sim 100$ MeV and during the same time the non-zero chemical potential remains in plasma. The value of k at which the evolution stops can be determined via (18) with $\gamma(\eta) \sim 1$. We find that $k \approx k_{\max}(\eta)$ – the wave-number at which the spectrum is peaked at the moment η is of the order of final time, determined by (17), i.e. $\eta_\sigma(k_{\max}(\eta)) \sim \eta$. Thus the value of k_{\max} is approximately the same as in the standard MHD case, when all modes with $\eta_\sigma(k) < t$ would be erased by the magnetic diffusion. *However*, the total energy of the spectrum (or, equivalently $\mathcal{H}_{k_{\max}}$ is much higher in our case – the presence of chemical potential allows for an “inverse cascade” process – the energy stored in short wave-lengths modes to be transferred to the longer wave-lengths (as Fig. C1).

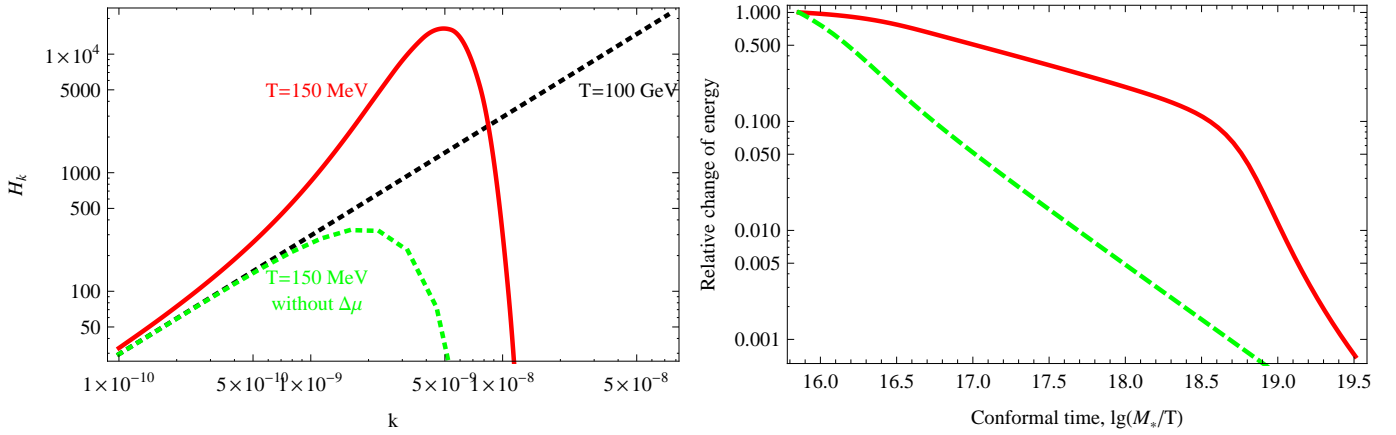


FIG. C1: **Left:** Initial helicity spectrum $\mathcal{H}_k^0 \propto k$ (black dotted line), the evolved spectrum \mathcal{H}_k at $T \approx 150\text{ MeV}$ when $\gamma = 1$ (red solid line) as well as the helicity spectrum evolved *solely* due to the magnetic diffusion (green dashed line) for $r_B \approx 5 \times 10^{-5}$. **Right:** The relative change of the total energy with (red, solid) and without (green, dashed) the chemical potential difference.

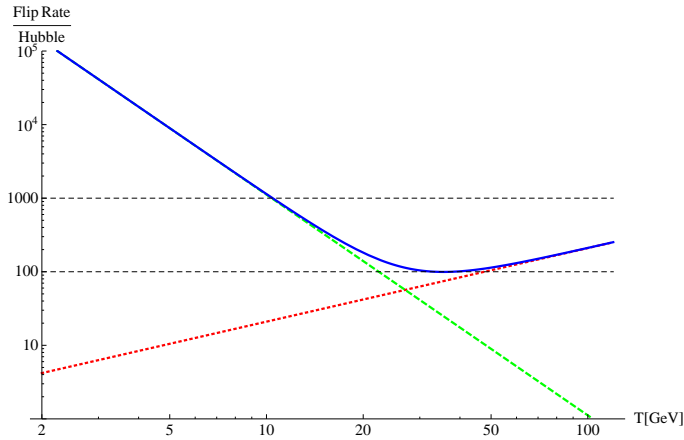


FIG. D1: Ratio of chirality-flipping rates to the Hubble rate for T in GeV range (blue solid line). Red dashed line is the flipping rate due to weak reactions, and green (dotted) is the rate due to electromagnetic processes.

Appendix D: Perturbative chirality flipping rates

Fig. D1 shows the ratio of perturbative chirality-flipping rates due to weak or electromagnetic reactions to the Hubble expansion rate (as a function of time).

Appendix E: Derivation of equations for \mathcal{H}_k

In this Appendix we provide the details of derivation of Eqs. (6)–(7).

Due to 3d translation and rotation invariance, we define the Fourier modes B_k and A_k for the magnetic field and its gauge potential in the usual way

$$B(x) = \int \frac{d^3k}{(2\pi)^3} e^{ik \cdot x} B_k \quad (\text{E1})$$

and introduce *magnetic helicity density* \mathcal{H}_k and *magnetic energy density* ρ_k in the k -space:

$$\mathcal{H}(\eta) = \int \frac{d^3k}{(2\pi)^3} \vec{A}_k \cdot \vec{B}_k^* \equiv \int dk \mathcal{H}_k \quad (\text{E2})$$

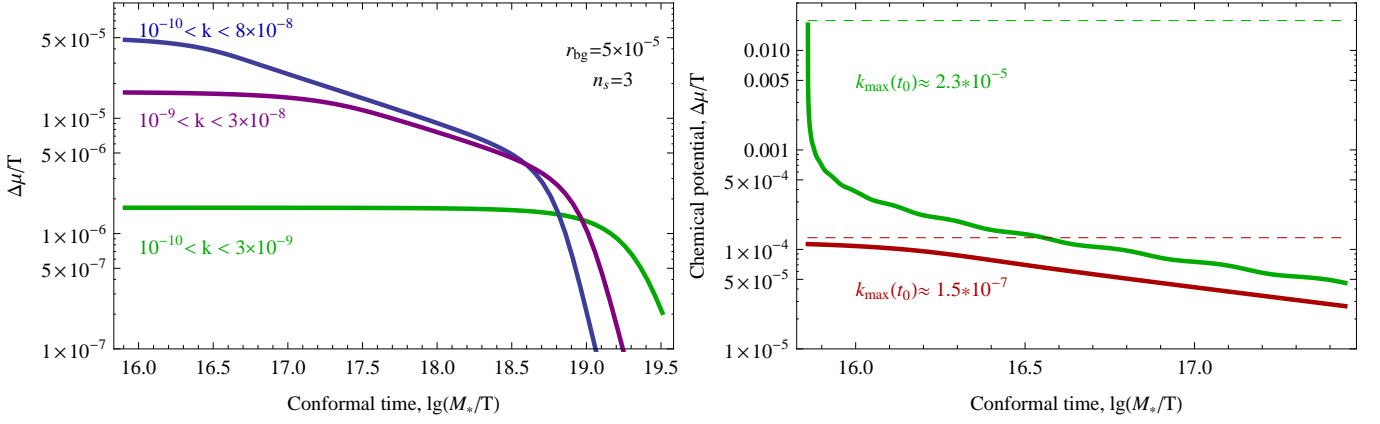


FIG. F1: **Left:** Evolution of $\Delta\mu$ for two spectra with the same total energy density $r_B \approx 5 \times 10^{-5}$, the same initial spectral index $n_s = 3$, and **different range of initial k** . $\lg \eta_\sigma = 18.7$ (green), $\lg \eta_\sigma = 16.7$ (purple). **Right:** Zoom on initial region of evolution of $\Delta\mu$ for two spectra with the same total energy density $r_B \approx 1$ and the same initial spectral index ($n_s = 5$) but **different range of initial k** over which this energy is distributed.

$$\rho_B \equiv \frac{1}{2V} \int \frac{d^3k}{(2\pi)^3} |\vec{B}_k|^2 = \int dk \rho_k \quad (\text{E3})$$

($\vec{B}_k^* = \vec{B}_{-k}$ as B is real). Notice that definitions of \mathcal{H}_k and ρ_k in Eqs. (E2)–(E3) contain integrals over the absolute value of the 3-vector k only (cf. [18–20]). Multiplying Fourier version of Eq. (5) by the complex-conjugated mode \vec{B}_k^* , we get:

$$\dot{\vec{B}}_k \vec{B}_k^* + \dot{\vec{B}}_k^* \vec{B}_k = -\frac{2k^2}{\sigma_c} \vec{B}_k^* \vec{B}_k + i \frac{2\alpha}{\pi} \frac{\Delta\mu}{\sigma_c} \vec{B}_k^* \cdot (\vec{k} \times \vec{B}_k) \quad (\text{E4})$$

With the use of $\vec{B}_k = i\vec{k} \times \vec{A}_k$ we obtain from Eq. (E4):

$$\frac{\partial \rho_k}{\partial \eta} = -\frac{2k^2}{\sigma_c} \rho_k + \frac{\alpha}{2\pi} \frac{\Delta\mu}{\sigma_c} k^2 \mathcal{H}_k \quad (\text{E5})$$

$$\frac{\partial \mathcal{H}_k}{\partial \eta} = -\frac{2k^2}{\sigma_c} \mathcal{H}_k + \frac{2\alpha}{\pi} \frac{\Delta\mu}{\sigma_c} \rho_k \quad (\text{E6})$$

If fields are maximally helical, i.e. $\rho_k = \frac{k}{2} \mathcal{H}_k$, Eq. (E5) reduces to (6).

Appendix F: Dependence on the parameters of the initial spectrum

Figs. F1 show the dependence of the chemical potential difference on the range of modes k in the spectrum.

Appendix G: Notations

1. Magnetic energy density

In this Appendix we discuss several conventions of expressing the energy density of the magnetic field $\rho_B = \frac{1}{2V} \int d^3x B^2$, used in the literature.

One possibility (used in this paper) is to express it in terms of the total radiation energy density

$$\bar{\rho} \equiv \frac{\pi^2}{30} g_* T^4 \quad (\text{G1})$$

Alternatively, one can express ρ_B in terms of the total entropy of radiation $\bar{s} = \frac{2\pi^2}{45}g_*T^3$ as follows (cf. [18]):

$$r_g \equiv \frac{\rho_B}{\bar{s}^{4/3}} \quad (\text{G2})$$

To convert between the r_B and r_g one can use:

$$r_g \approx \frac{r_B}{g_*^{1/3}} \approx 0.2r_B \left(\frac{100}{g_*} \right)^{1/3} \quad (\text{G3})$$

2. Dimensionless quantities

Eqs. (4–5) do not change in the expanding universe with FRW metric: $ds^2 = -dt^2 + a^2(t)d\vec{x}^2 = a^2(\eta)(-d\eta^2 + d\vec{x}^2)$, provided that we work with conformal coordinates x , use (dimensionless) conformal time $\eta = \frac{M_*}{T}$ (where we have used $a(t) = 1/T$ and neglected that g_* changes with time) and substitute $\Delta\mu, \sigma, T, \Gamma_f$ with their conformal counterparts $(\Delta\mu a), (\sigma a), (Ta), (\Gamma_f a)$, and introduce conformal electro-magnetic fields $E \rightarrow a^2 E = E_c, B \rightarrow a^2 B = B_c$. Notice that $\sigma a = \sigma_c \approx \text{const}$ [21]. We use these coordinates throughout the paper, starting from Eq. (8). To restore the dimensions it is sufficient to change any quantity as follows: $\Delta\mu \rightarrow \Delta\mu/T, k \rightarrow k/T, \mathcal{H}_k \rightarrow \mathcal{H}_k/T^3, \rho_k \rightarrow \rho_k/T^4$, etc.